Author Manuscript

Author Manuscript

Author Manuscript

Author Manuscript

HHS Public Access

Author manuscript

Cancer Res. Author manuscript; available in PMC 2021 May 15.

Published in final edited form as:

Cancer Res. 2020 November 15; 80(22): 5121–5133. doi:10.1158/0008-5472.CAN-19-3883.

Modeling Resistance and Recurrence Patterns of Combined Targeted-Chemoradiotherapy Predicts Benefit of Shorter Induction Period

David M. McClatchy III[1], **Henning Willers**[1], **Aaron N. Hata**[2,3], **Zofia Piotrowska**[2,3], **Lecia V. Sequist**[2,3], **Harald Paganetti**[1], **Clemens Grassberger**[1]

[1]Department of Radiation Oncology, Massachusetts General Hospital, Boston MA

[2]Department of Medicine, Harvard Medical School, Boston MA

[3]Massachusetts General Hospital Cancer Center, Charlestown, MA

Abstract

Optimal integration of molecularly targeted therapies such as tyrosine kinase inhibitors (TKI) with concurrent chemotherapy and radiation (CRT) to improve outcomes in genotype-defined cancers remains a current challenge in clinical settings. Important questions regarding optimal scheduling and length of induction period for neoadjuvant use of targeted agents remain unsolved and vary among clinical trial protocols. Here we develop and validate a bio-mathematical framework encompassing drug resistance and radiobiology to simulate patterns of local versus distant recurrences in a non-small cell lung cancer (NSCLC) population with mutated epidermal growth factor receptor (EGFR) receiving TKI and CRT. Our model predicted that targeted induction before CRT, an approach currently being tested in clinical trials, may render adjuvant targeted therapy less effective due to proliferation of drug-resistant cancer cells when using very long induction periods. Furthermore, simulations not only demonstrated the competing effects of drug-resistant cell expansion versus overall tumor regression as a function of induction length, but also directly estimated the probability of observing an improvement in progression-free survival at a given cohort size. We thus demonstrate that such stochastic biological simulations have the potential to quantitatively inform the design of multimodality clinical trials in genotype-defined cancers.

Introduction

Therapies targeting specific oncogenic driver mutations have dramatically improved survival in patients with metastatic cancer across several disease sites. Most significantly, tyrosine kinase inhibitors (TKIs) have become a standard-of-care treatment for metastatic non-small cell lung cancer (NSCLC) harboring mutations in the epidermal growth factor receptor (EGFR) (1, 2). Unfortunately, disease inevitably recurs as both pre-existing drug resistant

Corresponding Authors: David M McClatchy III, Massachusetts General Hospital, 55 Fruit St, Boston MA 02114. Phone: 617-643-6370; DMCCLATCHY@mgh.harvard.edu and Clemens Grassberger, Massachusetts General Hospital, 55 Fruit St, Boston, MA 02114. Phone: 617-724-1202; Grassberger.Clemens@mgh.harvard.edu.

No potential competing interests are declared by the other authors.

Author Manuscript Author Manuscript Author Manuscript Author Manuscript

cells and acquired *de-novo* drug resistant cells, mutating from drug-tolerant "persistent" cells during the course of treatment, outcompete the drug sensitive cells, thus manifesting the evolution of drug resistant tumors (3–6). In contrast to metastatic EGFR-mutant NSCLC, the role of TKIs in locally advanced (LA), non-metastatic NSCLC remains unknown. But, the addition of TKIs to-standard of-care concurrent chemotherapy and radiation (CRT) in patients with EGFR-mutant cancers has the potential to improve long term survival in this cohort. The recent PACIFIC trial has demonstrated the dramatic benefit that integration of new systemic agents can yield in LA-NSCLC (7): using adjuvant durvalumab, an anti-PD-L1 checkpoint immunotherapeutic agent, and standard-of-care CRT improved progression-free and overall survival significantly. However, there was no benefit to immunotherapy over chemotherapy in the subset of EGFR-mutant patients (8). Therefore, the PACIFIC trial exemplifies not only the possible benefits of including successful systemic agents into earlier stages of NSCLC treatments, but also the considerable but underutilized potential TKIs may play in the increasing number of successful treatment options for EGFR-mutant LA-NSCLC.

However, it is entirely unknown how to optimally administer TKIs with CRT in order to minimize the risk of acquired drug resistance and improve the efficacy of CRT. Consequently, the design of these multimodality therapy trials is largely empirical with great variability in treatment protocols and a "one-size fits all" approach. Additionally, a large part of the treatment design space is not explored due to the infeasibility of running randomized controlled trials for every possible combination of treatments.

One useful method to sample treatment design space is bio-mathematical modeling, which enables the quantitation of abstract, interconnected phenomena making it a powerful tool in the field of translational oncology for both hypothesis testing and generation (9, 10). Specifically, mathematical modeling of tumor evolution has significantly impacted our understanding and interpretation of acquired resistance to targeted cancer therapies (11, 12) and has helped formulate the idea of collateral sensitivities to sequential drug regimens (13). Additionally, combing evolutionary modeling of tumors with mechanistic biological models of radiation cell kill and plasma level drug concentrations has enabled novel dosing schedules of radiation therapy in glioblastoma (14), intercalated administration of multiple targeted and chemotherapy agents for melanoma (11), and novel pulsed injections of TKI therapy in EGFR-mutant NSCLC (15). This TKI delivery protocol designed using mathematical modeling was successfully translated into a clinical trial (15, 16).

In this study, we present a generalized bio-mathematical model to optimize TKI plus CRT multimodal regimens in EGFR-mutant LA-NSCLC, with a focus on the relative effect of therapy on local versus occult distant disease sites. In metastatic EGFR-mutant NSCLC populations, TKIs result in significant improvements in overall response and survival compared to chemotherapy, but acquired drug resistance inevitably leads to disease recurrence (1–6, 17). Optimal combination regimens with EGFR TKIs and CRT for LA-NSCLC patients have not yet been studied. A major complicating factor is that failure after CRT can be local or distant, which may be differentially impacted by TKIs. The goal of this study is to inform the design of TKI-CRT multimodal clinical trials through mechanistic, bio-mathematical modeling, which encompasses fundamental principles of evolutionary

Author Manuscript Author Manuscript Author Manuscript Author Manuscript

targeted drug resistance, radiation biology, and comorbidities. The model aims at quantitative, *in-silico* analyses of varying treatment design parameters to predict effect sizes in heterogeneous patient populations, and also the probability of observing such effects at a given sample size. We achieve this by defining distributions for model parameters to simulate inter-patient heterogeneity, calibrating our model using several institutional datasets, and subsequently demonstrate accurate model predictions of recurrence rates in independent validation datasets of recent multicenter clinical trials and meta-analyses. Next, we exhaustively explore the multimodal treatment design space and show that a TKI induction period of 2–3 months, as used in the recent clinical trials NCT01553942 and NCT01822496, may reduce the effectiveness of adjuvant TKI therapy due to the proliferation of TKI resistant clones during the induction period. Instead, we propose and provide a quantitative rationale for an individualized induction period tailored to resistance evolution. This mathematical framework can not only inform the design of future multimodal TKI-CRT trials, but also be extended to other oncogene driven cancers to design more precise and personalized cancer treatment regimens.

Materials and Methods

Local and Distant NSCLC Progression Model

Our tumor progression model is an advancement of our previously published bio-mathematical models of CRT in NSCLC (18) and evolutionary TKI resistance in advanced EGFR-mutant NSCLC (12). An exponential vector system (Eqs. 1–14) tracked the number of TKI resistant, drug-tolerant persistent, and sensitive clonogenic cells (clonogens). While TKI sensitive clonogens are killed by the drug and TKI resistant clonogens multiply irrespective of drug exposure, drug-tolerant persistent clonogens neither proliferate or succumb to the drug, but do mutate in drug resistant clonogens (4, 5). The tumor burden was separated into local versus distant compartments to deconvolve in-field locoregional failures and out of field distant failures. Thus, time to local and distant failures (See Suppl. Eqs. S5–S6) were directly modeled from the local and distant cell compartments respectively, rather than modeling overall survival as a function of total tumor burden. This was an important distinction as post-progression treatment in the era of targeted therapy can be highly patient specific with varying degrees of response (19). Comorbidity related deaths were implemented into our model with a Monte Carlo Russian Roulette formalism (See Suppl. Eqs. S1–S4) and estimated from an analysis of the Surveillance, Epidemiology, and End Results (SEER) Program for a regional lung cancer population (20, 21). While a recent SEER analysis demonstrated that lung cancer patients receiving TKIs were less likely to be smokers, TKI recipients did not have a statistically significant difference in comorbidity as measured by the Charlson comorbidity index (0 vs. 1+) (22). Progression was defined as the first occurring local failure, distant failure, or comorbidity related death. A pictorial summary conceptualizing the model and its main endpoints is shown in Fig. 1.

Model Calibration to Recurrence Dynamics of NSCLC

While the tumor progression model tracked a single tumor volume trajectory, a general patient population with heterogeneity in their presentation, response to treatment, and recurrence patterns was simulated by creating truncated normal and truncated log-normal

Author Manuscript Author Manuscript Author Manuscript Author Manuscript

distributions for the model parameters as was done previously (18). These distributions were then randomly sampled for each run (i.e. simulated patient) of the tumor progression model, yielding a histogram of times to events, which in turn was used to create simulated Kaplan-Meier (K-M) curves for the distributed population (see Suppl. Note). The model parameter distributions were then optimized such that the model predicted K-M curves matched clinically reported K-M curves, as was done in Geng et al. (18). In this work, the growth and radiosensitivity distributions were fitted to literature K-M curves of freedom from local and distant failure (FFLF and FFDF) in wildtype (WT) and EGFR-mutant locally advanced NSCLC populations receiving definitive concurrent CRT (19, 23, 24). The TKI model parameters were derived from a model-based analysis of advanced EGFR-mutant NSCLC patients (see Suppl. Note). A full summary of the optimized model parameters along with the source of the calibration data is shown in Table 1.

While the 2 yr. FFLF for wild-type (WT) NSCLC has been shown to be relatively poor in the range of [54–63] %, EGFR-mutant tumors have a noticeably better response with a 2 yr. FFLF in the range [70–87] % (19, 23, 24). This differential response in FFLF was observed after CRT alone and the results were not confounded by TKI administration. Furthermore, *in-vitro* studies have demonstrated an enhanced radiosensitivity of EGFR-mutant NSCLC compared to WT (25), and so in our model unique radiosensitivity distributions were defined for WT and EGFR-mutant populations separately and optimized against FFLF. Distant metastases have been observed to be the most common form of recurrence with a 2 yr. FFDF in the range of [31–43] % with no statistically significant relationship to EGFR status (19, 23, 24). Therefore, a common metastatic fraction and growth rate distribution were defined for both populations and optimized against FFDF, as shown in Fig. 2. For each calibration step, two parameters were optimized simultaneously using brute force, and while each two parameters exhibited a correlative relationship, a global solution was determined (Suppl. Fig. 1(A–F)). The bootstrapped confidence intervals encompassed these correlative regions, and model predicted failure rates matched the calibration data over these intervals (Suppl. Fig. 1(G–L)).

The model predicted FFDF curve for the optimal growth and metastatic fraction parameters is shown in Fig. 2(A) and exhibited a strong correlation to the weighted mean of the literature reported values (r^2>0.99, p=0.002, Fig. 2(D)). Similarly, the model predicted FFLF curves with the optimized WT and EGFR-mutant radiation sensitivity distributions matched the literature reported values as shown in Fig. 2(B) and (C), respectively. For both populations, the model predicted FFLF were similarly strongly correlated with reported values (r^2>0.97, p<0.02, Fig. 2(E) and (F)). Additionally, the model predicted PFS was calculated with the optimized parameters for WT and EGFR-mutant populations, which yielded only a minor increase in PFS for the more radiosensitive EGFR-mutant population (HR = 1.06 CI, 1.02–1.09, Suppl. Fig. 2). This was in accordance with literature reported observations of a lack of statistically significant difference in time to first recurrence between the WT and EGFR-mutant populations (19, 24).

Author Manuscript Author Manuscript Author Manuscript Author Manuscript

Guide to Model Equations and Assumptions

Mathematical Implementation of Local versus Distant Tumor Progression Model

We described the evolution of the number of TKI resistant (N_R), persistent (N_P), or sensitive (N_S) clonogens in the distant (N_D) or local (N_L) compartments (Eqs. 5–10) with exponential factors accounting for the differential terms of Gompertzian cell growth, Norton-Simon cell kill by TKIs, log cell kill by chemotherapy, and linear-quadratic (LQ) radiation cell kill (with the assumption of $\alpha/\beta = 10$). While older reports suggested α/β could be higher than 10 for lung cancer (26), our results were insensitive to the exact value of α/β as different fractionation schema were not considered. Additionally, the efficacy of chemoradiation was assumed to be independent of the proximity to TKI administration, i.e., the model parameters associated with chemoradiation cell kill are considered to be constant throughout the treatment. The initial local cell number was based on tumor volume distributions for each stage of NSCLC and an assumed cell density of 5.8×10^8 cells/cm^3 estimated from previous model based work of NSCLC tumor growth (18, 27). The initial distant cell number was assumed to be a scalar fraction (f_{met}) of the initial local cell number (Eq. 2), which was fitted during the modeled calibration procedure. Time of distant failure was defined as the distant compartment reaching a PET-detectable volume of 1 cm^3 (28), i.e. when $N_{D_{total}}(t) > 1cc$ (Eqs. S6). Time of local failure was defined as growth of the local compartment past its size at the start of treatment, i.e. when $N_{L_{total}}(t) > N_{L_{total}}[0]$ (Eqs. S5).

By heuristically simulating a patient population, yielding histograms of time to failures, time-varying rates of freedom from local and distant failures were modeled. Throughout treatment and regrowth, there was also a transitional term to account for acquired mutations from TKI persistent to resistant cells with the mutation rate μ assumed to be 10^{-7} based upon in-vitro studies of TKI resistance (29). The model also assumed that the growth of the persistent compartment was slowed during TKI administration as seen clinically (Eq. 13) (5, 12). The first order pharmacokinetic model of chemotherapy (C_C, Eq. 12) and TKI plasma concentrations (C_{TKI}, Eq. 14) used in our model were fully described in previous publications (12, 18, 30). The TKI dosing regimen of a single daily dose was implemented for both induction and maintenance, as is done clinically (NCT01553942). The state equations were implemented over 1 day time periods with 0.1 day resolution (Δt), and with the differential effect of each term calculated independently. Discrete treatment events, such as radiation delivery or a bolus injection of chemotherapy, were assumed to occur instantaneously at a single timepoint (Eq. 11–12). At a discrete time step, if a cell compartment went below 1 cell, it was assumed to be controlled and set to 0. A total of 5 iterations of 1024 patients (n=5120) were simulated for the calibration of model parameters, while a total of 1024 patients having 12 unique combinations of initial resistant and persistent fractions (n=12288) were simulated for the model validation and multimodal treatment outcome predictions. The effect of simulated population size on variability of outcomes is examined in the simulated in-silico induction trial section of the Results.

Software Implementation

The simulations were implemented in Python *v3.7* using both the *SciPy v1.3.1* (31) and *NumPy v1.17.2* (32) libraries. The *scipy.odeint* routine was used to implement TKI therapy

Author Manuscript Author Manuscript Author Manuscript Author Manuscript

and growth terms, while CRT was implemented exponentially. The *seaborn v0.9.0* python library (33) was used to present data, and the *lifelines v0.24 python* library (34) was used for the survival analysis (see Suppl. Note). The source code for the simulations and resulting data are available at github.com/bomcclatchy/Modeling-Multimodal-TKI-ChemoRadiation.

$$t = k\Delta t \qquad N_{D_{tot}}[0] = f_{met} \cdot N_{L_{tot}}[0] \qquad N_{D_{tot}} = N_{D_S} + N_{D_P} + N_{L_R} \qquad N_{L_{tot}} = N_{L_S} + N_{L_P} + N_{L_R} \tag{1-4}$$

Distant Compartment

$$N_{D_S}[k+1] = N_{D_S}[k] * \exp\left\{(1 - \beta_{TKI} C_{TKI}[k]) \cdot \rho \Delta t \cdot \log\left(\frac{K}{N_{D_{tot}}[k]}\right) - \sum_{agents,i} \beta_i C_i[k]\right\} \tag{5}$$

$$N_{D_P}[k+1] = N_{D_P}[k] * \exp\left\{(1 - \mu) \cdot \rho_P[k] \Delta t \cdot \log\left(\frac{K}{N_{D_{tot}}[k]}\right) - \sum_{agents,i} \beta_i C_i[k]\right\} \tag{6}$$

$$N_{D_R}[k+1] = N_{D_R}[k] * \exp\left\{\left(\rho + \rho_P \frac{N_{D_P}[k]}{N_{D_R}[k]} \mu\right) \cdot \Delta t \cdot \log\left(\frac{K}{N_{D_{tot}}[k]}\right) - \sum_{agents,i} \beta_i C_i[k]\right\} \tag{7}$$

Local Compartment

$$N_{L_S}[k+1] = N_{L_S}[k] * \exp\left\{(1 - \beta_{TKI} C_{TKI}[k]) \cdot \rho \Delta t \cdot \log\left(\frac{K}{N_{L_{tot}}[k]}\right) - \sum_{agents,i} \beta_i C_i[k] - (\alpha d[k] + \frac{\alpha}{10} d[k]^2)\right\} \tag{8}$$

$$N_{L_P}[k+1] = N_{L_P}[k] * \exp\left\{(1 - \mu) \cdot \rho_P[k] \Delta t \cdot \log\left(\frac{K}{N_{L_{tot}}[k]}\right) - \sum_{agents,i} \beta_i C_i[k] - (\alpha d[k] + \frac{\alpha}{10} d[k]^2)\right\} \tag{9}$$

$$N_{L_R}[k+1] = N_{L_R}[k] * \exp\left\{\left(\rho + \rho_P \frac{N_{L_P}[k]}{N_{L_R}[k]} \mu\right) \cdot \Delta t \cdot \log\left(\frac{K}{N_{L_{tot}}[k]}\right) - \sum_{agents,i} \beta_i C_i[k] - \left(\alpha d[k] + \frac{\alpha}{10} d[k]^2\right)\right\} \tag{10}$$

$$d[k] = \begin{cases} 2\ Gy & k \text{ during radiation delivery} \\ 0 & \text{else} \end{cases} \qquad C_C[k+1] = \begin{cases} \hat{C}_{C,bolus}[k_{C,bolus}] \left(\frac{1}{2}\right)^{((k-k_C)\Delta t / t_{1/2})} & k \text{ during chemotherapy} \\ 0 & \text{else} \end{cases} \tag{11,12}$$

$$\rho_P[k] = \begin{cases} \rho/4 & k \text{ during TKI} \\ \rho & \text{else} \end{cases} \qquad C_{TKI}[k+1] = \begin{cases} (\hat{C}_{TKI,daily}[k_{TKI,daily}] + C_{TKI}[k]) * \exp\{-\kappa \Delta t\} & k \text{ during TKI} \\ 0 & \text{else} \end{cases} \tag{13,14}$$

Results

Retrospective Model Validation Against Clinical Trial Outcomes

With all of the model parameters calibrated and fixed, the tumor progression model was then validated against independent data sets from multi-institutional phase 3 trials of either TKI alone or CRT alone (see Suppl. Note). First, the model predicted PFS in an advanced stage IV population was compared against the TKI arm of the EURTAC trial, which compared chemotherapy versus TKI in advanced EGFR-mutant NSCLC (Fig. 3(A)) (1). A recent meta-analysis of first generation TKIs in EGFR-mutant advanced NSCLC found the EURTAC trial to have the most similar effect to the median of the six analyzed trials (HR EURTAC = 0.42, CI, 0.27–0.64, HR median = 0.37, CI, 0.27–0.52) making it an appropriate benchmarking dataset (17). The model predicted PFS was similar to the trial reported PFS (r^2=0.92, p<1e-5, Fig. 3(B)), validating the rate of progression during TKI administration as predicted by the model. A waterfall plot of the maximum change in tumor volume from baseline is shown for a simulated patient population (n=256) in Fig. 3(C), with each bar color-coded by degree of initial TKI resistance. From an analogous waterfall plot reported in the EURTAC trial, we see that the trial and the model simulated populations have similar tumor response dynamics with a median tumor volume decrease of 50%−75% and <10% of patients exhibiting progressive disease, demonstrating the validity of the derived TKI model parameters. Furthermore, the capacity of the model to stochastically embody a heterogeneous population is shown in Fig. 3(C), as tumor shrinkage was not simply a function of pre-existing resistance but was modulated by other factors such as growth rate.

Next, model predicted PFS for a WT LA-NSCLC population receiving concurrent CRT was compared against the results of the PROCLAIM trial (35), representing the pre-PACIFIC

Author Manuscript Author Manuscript Author Manuscript Author Manuscript

standard of care for CRT alone (Fig. 3(D)). Model predicted PFS for concurrent CRT correlated very strongly to the aggregated reported PFS of the trial (r^2>0.99, p<1e-21, Fig. 3(E)), validating the absolute rate of recurrences during concurrent CRT as predicted by the model. Additionally, the model predicted local and distant failure dynamics for sequential versus concurrent CRT was in accordance with the results of a meta-analysis of six randomized trials comparing chemotherapy scheduling in LA-NSCLC (36). The model accurately predicted a significant benefit in local failure rates for concurrent CRT with a modeled HR of 0.79 (CI, 0.77–0.82), while the meta-analysis reported a HR of 0.77 (CI, 0.62–0.95, p=0.01) (Suppl. Fig. 3(A)). Furthermore, the model predicted no difference in distant failure rates for sequential versus concurrent CRT (HR = 1.00, CI, 0.97–1.03), which was consistent with the findings of the meta-analysis that there was no statistically significant effect of chemotherapy scheduling on distant failure rates (HR = 1.04, CI, 0.86–1.25, p=0.69) (Suppl. Fig. 3(B)). Together, these results provide strong evidence for the validity of the model predicted local and distant recurrence patterns during various treatment schedules as compared to current NSCLC multicenter clinical trials.

Estimation of Improved Outcomes for TKI Induction and Maintenance

With the same simulated patient population and treatment parameters used during model validation (histograms shown in Suppl. Fig. 4), the expected recurrence dynamics of combining CRT and TKI therapy were explored. Two main treatment designs were simulated for locally advanced EGFR-mutant NSCLC: TKI induction with daily administration up to 16 weeks, followed by definitive concurrent CRT, followed with or without adjuvant TKI maintenance. These two treatment schemes were chosen to approximate the format of ongoing combined TKI+CRT trial protocols (see Suppl. Note). TKI therapy concurrent with CRT was not modeled as initial clinical experience suggests the potential for increased toxicity and also non-synergistic efficacy (37, 38). The hypothesis explaining these results was that TKIs cause G1 cell-cycle arrest stunting cell replication antagonizing both chemotherapy and radiotherapy (39, 40), despite both agents having cytotoxic effects regardless of cell-division.

The predicted 2 yr., 3 yr., and 5 yr. FFLF, FFDF, and PFS as a function TKI induction length with and without adjuvant TKI maintenance are plotted in Suppl. Fig. 5(A), (B), and (C), respectively, while the endpoints over the entire design space are tabulated in Suppl. Fig. 6. For TKI induction without maintenance, the greatest predicted benefit for FFLF, FFDF, and PFS over CRT alone occurred with 2 wks. of induction (Δ5 yr. FFLF 1.5%, Δ5 yr. FFDF 11.1%, Δ5yr. PFS 6.5%), with a decreasing benefit as the induction length increased resulting in a similar predicted outcome to CRT alone with 16 wks. of induction. For each endpoint, there was a predicted additive benefit for including adjuvant TKI maintenance to induction regardless of the time point or duration of the induction period (Suppl. Fig. 5). But, the greatest benefit of including TKI maintenance was seen at shortest induction periods (Δ5yr. FFLF 5.8%, Δ5yr. FFDF 23.7%, Δ5yr. PFS 15.8% with 0 wks. induction and Δ5yr. FFLF 3.5%, Δ5yr. FFDF 7.7%, Δ5yr. PFS 6.7% with 2 wks. induction compared to CRT alone), with outcomes monotonically worsening as a function of induction length for each endpoint. The local failure rate was the least sensitive to the length of induction, given the high radiosensitivity and local control rates of EGFR-mutant NSCLC. The most

Author Manuscript Author Manuscript Author Manuscript Author Manuscript

dramatic effects were seen in the distant failure rates, which have an enhanced sensitivity to the evolutionary dynamics during induction as the subsequent chemotherapy was the only modeled therapeutic able to target the occult TKI resistant subpopulation in the distant compartment.

Longer Induction is Predicted to Induce TKI Resistance

The maximum benefit observed with 2 wks. of TKI induction when maintenance was not administered is due to the fact that this time point presents a balance in benefit for both responders and non-responders: if a patient does not respond at all there is not much additional growth that early, while the responders will have at least derived some benefit through volume shrinkage. Furthermore, the benefit of delaying progression by means of extending the induction length (≥ 4 wks.) was gradually outweighed by the proliferation of the resistant population and resulting tumor volume increase prior to CRT. But surprisingly, when adjuvant maintenance was administered, the shortest induction periods were predicted to have the lowest local and distant failure rates. This suggests that the relative benefits of shrinking the tumor volume before CRT with TKIs was outweighed by the cost of acquired TKI resistance caused by targeted evolution during induction, which dramatically reduced the efficacy of TKI maintenance. This tradeoff in competing advantages of tumor size and TKI sensitivity is exemplified in the Kaplan-Meier analysis and simulated tumor volume trajectories displayed in Fig. 4.

The median tumor volume trajectory stratified by TKI sensitive, persistent, and resistant cell subtypes receiving 2 and 12 wks. of TKI induction with adjuvant maintenance are plotted for the local compartment in Fig. 4(A) and the distant compartment in Fig. 4(B). While both treatment schedules resulted in local control (Fig. 4(A)), a 2 wk. induction resulted in control of the initially microscopic resistant subpopulation of the distant compartment with chemotherapy during CRT and a slow regrowth of the persistent subpopulation during maintenance (Fig. 4(B)). But over the course of the longer 12 wks. of induction, the resistant subpopulation of the distant compartment out competed and outgrew the slowly proliferating persistent subpopulation, resulting in a rapid, resistant distant recurrence after ~1 yr. of adjuvant TKI therapy (Fig. 4(B)), controlling for the same efficacy of chemotherapy during CRT. Additionally, the resistant growth during induction was accelerated in the distant compartment compared to the local compartment because of the resource advantage at lower cell numbers inherently modeled with Gompertzian growth (12).

Kaplan-Meier curves for the simulated FFLF, FFDF, and PFS for various TKI induction and maintenance schedules show the long term predicted benefit over CRT alone in Fig. 4(D), (E), and (F), respectively. While TKI induction and maintenance was predicted to have modest FFLF benefit over CRT alone, there was little stratification between different induction lengths (Fig. 4(D)). But for FFDF (Fig. 4(E)) and PFS (Fig. 4(F)), there was a much stronger effect with greater stratification between induction lengths. However, stratification between induction lengths was not observed until ~1 yr. after the start of treatment, due to the time needed for distant cells to proliferate to an observable threshold after CRT. In this analysis, a schedule of no induction with CRT and adjuvant TKI maintenance was not considered despite having the best predicted outcomes, as some

Author Manuscript Author Manuscript Author Manuscript Author Manuscript

amount of induction with a measurable response in tumor volume is needed to warrant daily TKI administration after CRT until progression.

Calculated hazard ratios for 2 wks., 8 wks., and 12 wks. of TKI induction with adjuvant maintenance quantified the relative effect size of each multimodal treatment schedule compared to CRT alone, independent of the simulated sample size. As shown in Fig. 4(C), FFDF had the most dramatic effect size, having a hazard ratio of 1.89 (CI, 1.83–1.96) for 2 wks. induction dropping to 1.38 (CI, 1.34–1.43) for 12 wks. induction. The expected statistical significance of these proposed treatment schema at clinically relevant sample sizes were stochastically investigated, as described in the next section.

Statistical Significance and Power in a Model-Based Trial Design

Evaluating the statistical significance between the predicted failure rates of different treatment arms was a non-trivial task as an arbitrarily large number of patients can be simulated, which could result in statistical significance even when hazard ratios were very close to one. Therefore, we determined the probability of reaching a certain level of statistical significance as a function of the number of trial patients. We utilized the stochastic nature of the model by randomly sampling multiple iterations of simulated patients in order to yield an estimate of the false negative rate at lower sample sizes and the corresponding statistical power (see Suppl. Note). Doing so, our model based analysis not only yielded an expected magnitude of effect between two multimodal treatments but also quantified the probability of observing the effect in a population of a given size.

A simulated two armed clinical trial of 2 wks. versus 12 wks. of TKI induction with CRT and adjuvant TKI maintenance was modeled with FFDF as the endpoint, which has both the strongest effect (Fig. 4(F)) and is particularly relevant for future targeted therapy trials given the relatively high rates of local control in NSCLC with CRT for EGFR-mutant patients. An induction length of 2 wks. was chosen for arm 1 as it was predicted to improve outcomes and also would allow to screen for initial TKI response. For arm 2, 12 wks. of induction was chosen to mimic an induction length currently investigated (NCT 01822496). A depiction of the simulated evolution of TKI resistance illustrating the hypothesized mechanism of benefit to a shorter induction period is shown in Fig. 5(A). Modeled FFDF K-M curves displayed a constant magnitude of effect but wider confidence intervals with decreased sample size (Fig. 5(B)). A heatmap of the log-rank p-values testing the significance between the two arms over 1000 iterations revealed the variability in detecting the effect with fewer patients in Fig. 5(C). This was further quantified in Fig. 5(D), where the distributions of median FFDF in each arm have a consistent mean but increasing variance with decreasing sample size. Note that the simulation ran for 5 yrs. and so the peak at 60 months can be attributed to iterations where the median FFDF was not yet reached. The distribution of log-rank p-values between the arms for the 1000 iterations is shown in Fig. 5(E) along with the median p-values. The fraction of iterations reaching statistical significance of 0.05 was estimated to be the statistical power, and is plotted as function of sample size in Fig. 5(F). Thus, this analysis has projected that a clinical trial would need 256 patients per arm for a power of 79%.

Additionally, this benefit to a shorter induction period was seen regardless of the initial TKI sensitivity. When simulated patients were stratified by initial resistant or persistent fractions

Author Manuscript Author Manuscript Author Manuscript Author Manuscript

(see Suppl. Note), and the trial was re-run for each combination of Vr(0) and Vp(0), the 2 wk. arm always benefitted as quantified by the hazard ratio (Suppl. Fig. 7). While this benefit appeared to be short term for patients with higher levels of pre-existing persistence and lower levels of pre-existing resistance, a durable benefit was observed higher levels of pre-existing resistance and lower levels of pre-existing persistence.

A corresponding analysis using PFS as the endpoint is displayed in Suppl. Fig. 8(A–E), from which it was estimated that 512 patients per arm are needed to reach a power over 80%. While these analyses assumed a general population, the modeled population can be readily stratified into clinically distinguishable groups. For instance, modeled populations above and below the median initial tumor size (7.2 cm) will exhibit diverging distributions of predicted failure rates, which will consequently decrease and increase the required number of patients in each sub-population needed for an adequately powered clinical trial.

Discussion

We have developed a mathematical framework to forecast the relative effectiveness of user-defined regimens of combined targeted-chemoradiation therapy and have applied this methodology to optimize the multimodal administration of tyrosine kinase inhibitors in locally advanced NSCLC. This framework integrates fundamental principles of tumor growth, radiation biology, and acquired drug resistance, with model parameters calibrated to institutional outcomes and predicted recurrence rates independently validated against clinical trial outcomes. While our previous modeling work has exclusively investigated targeted (12) or cytotoxic (18) therapy, the current framework not only integrates both treatment modalities, but also deconvolves local versus distant failures, creates population based model parameters specific for EGFR-mutant patients, and includes stochastic non-cancerous failures. We predict local and distant recurrence rates for various lengths of TKI induction before CRT and estimate the expected number of patients needed to observe a clinical benefit. In contrast to the current design of multimodal clinical trials which prescribe 2–3 month long induction periods, we discover an inverse relationship between progression and length of induction. In this sense no induction period at all would be optimal. However, some TKI induction is indicated because tumor response to the TKI needs to be verified before proposing an adjuvant TKI regimen. Thus, we propose 2 weeks because a volumetric reduction at this point can be observed when measured by consistent volumetric segmentation.

After 2 weeks of TKI exposure, there may not be maximal macroscopic gross tumor volume change; however, at these early time points, the occult TKI resistant and persistent populations will still be microscopic and with greater potential for control by cytotoxic therapy. Even though we make the assumption that pre-existing resistant cells exist at therapy initiation, our result does not entirely depend on this assumption. Even assuming no pre-existing cells would favor shorter induction periods, as this reduces the probability of cells acquiring mutations that confer resistance. The sooner CRT is administered, the sooner the pool of possible persister cells that could acquire resistance is diminished, increasing the efficacy of the TKI maintenance regimen. Thus, the benefit to shorter induction periods holds true regardless of the absolute of effect of CRT, as long as the CRT has the ability to

Author Manuscript Author Manuscript Author Manuscript Author Manuscript

control non-sensitive TKI cells. This should also hold true for second and third generation TKIs as these drugs still result in acquired drug resistance through a combination of pre-existing and acquired mutations (3), despite overcoming the EGFR T790M mutation which has indeed resulted in superior PFS compared to first generation TKIs (2). Finally, the predicted benefit of a shorter induction period was robust to any assumed level of pre-existing TKI sensitivity in our model, but a greater benefit was seen in tumors with higher levels of pre-existing TKI resistance.

Our result that shorter induction times lead to better outcomes contradicts expectations in current multimodal trial protocols for LA-NSCLC, but reflects the increasing risk of TKI resistance as a function of TKI exposure. Induction before CRT has several benefits, most notably decreasing tumor size, which has been shown to improve overall survival when treated with CRT (41) and may also lead to surgical candidacy as outlined in the ASCENT trial protocol (NCT 01553942). But, upfront TKI exposure in advanced staged patients has resulted in a 50–75% average volume change (1), which is similar to the expected surviving fraction after a single 2 Gy radiation fraction (SF2Gy) in NSCLC (42). Additionally, upfront TKI exposure will extend the duration of treatment compared to CRT alone, which will ostensibly delay disease progression. But as patients systemically become resistant over the course of months, adjuvant TKI maintenance therapy may be rendered ineffective. Conversely, with upfront chemoradiation therapy and the ability to control TKI resistant cells, the adjuvant TKI maintenance has the potential to dramatically slow tumor regrowth. And in fact, a retrospective analysis of the treatment of brain metastases originating from EGFR-mutant NSCLC demonstrated that upfront radiotherapy with adjuvant TKIs nearly doubled overall survival compared to upfront TKIs until progression and subsequent radiotherapy (34.1 vs. 19.4 mo.; $p = .01$) (43). But in the locally advanced setting, some initial TKI exposure is needed in order to demonstrate tumor response before maintenance therapy can be considered. Furthermore, there is evidence to suggest that TKI exposure may prime the cells for radiotherapy by inducing senescence (44).

Genetic heterogeneity present throughout a patients' tumor predicates the clinically observable acquired treatment resistance (45). There are two main models explaining the mechanism by which intratumoral heterogeneity and consequently treatment resistance arises: (1) branched clonogenic evolution where subpopulations arise from an accumulation of mutations and (2) cancer stem cells (CSCs) that are predominantly dormant and treatment resistant, but uniquely give rise to the diversity of differentiated cancer cells (9, 46). Additionally, models have been proposed unifying CSCs and clonogenic evolution, suggesting that CSCs themselves can acquire favorable mutations leading to competing subpopulations (47). In this work, a form of clonogenic evolution was assumed with CSCs not explicitly modeled, as the focus of this analysis was acquired TKI resistance, which has been shown to occur through specific genetic mutations (5, 6). As such, our model assumes that TKI resistant cells have the same chemo- and radiosensitivity as TKI sensitive cells, which is in line with experimental evidence (25).

While our model does not explicitly account for the constricting effect of TKIs on vasculature, resource deprivation is implicitly modeled through the slowed growth of the TKI persistent subpopulations resulting in apparent stunted tumor growth. However,

Author Manuscript Author Manuscript Author Manuscript Author Manuscript

modeling based *in-vitro* and *in-vivo* studies have shown that alterations to microenvironment can modulate the growth of resistant and persistent sub-clonogens independently, which in turn can lead to frequency dependent tumor evolution (48, 49). Future work could incorporate the non-cell autonomous effects of vasculature modulation into the model, by both EGFR-TKIs and also anti-angiogenic vascular endothelial growth factor inhibitors (VEGF-TKIs) which have shown great synergy when administered in combination (50). While *in-vitro* studies have suggested that TKI exposure can modulate DNA repair pathways affecting chemoradiation sensitivity (51, 52), clinical studies have shown chemotherapy intercalated with TKIs to be effective (53) and recent reports have demonstrated effectiveness of radiation therapy after TKIs in oligometastatic disease (54). Consequently, the effects of sequential administration of TKIs and CRT were conservatively assumed to be independent. However, TKIs and CRT were not simulated concurrently as uncertainty regarding the interplay and potential toxicity of concurrent TKIs + CRT remains (37, 38), but could be investigated in future studies as robust clinical data becomes available. Furthermore, while we parameterized our model using the chemotherapy regimen in RTOG 9410, clinical experience has demonstrated similar outcomes with a variety of chemotherapy regimens (55).

Based on our framework, future modeling studies might aim at stratifying simulated populations (e.g. high or low radiosensitivity α, tumor growth ρ) and determine which patient populations experience the most benefit from shorter versus longer induction periods, thus further personalized therapy. Potential biomarkers for NSCLC radiosensitivity demonstrated to be associated with survival outcomes are rad51 expression (56) and the polygenic radiosensitivity index (RSI) (57, 58). Additionally, ki67 expression and fluorothymidine uptake imaged by positron emission tomography have both shown to be related to tumor cell proliferation and could be potential biomarkers of tumor growth rate (59). Additionally, future modeling work could focus on predicting organ specific distant failure rates in LA-NSCLC, as brain metastases are common in EGFR-mutant tumors and may be amenable to further radiation (43).

Our work shows the possible impact that mathematical modeling can have on clinical trials exploring the integration of new biological agents into current treatment approaches, a topic that has recently gathered increased attention (60). Mathematical models based on patient data have been used in the past to optimize radiation therapy (14) or to understand underlying disease dynamics (61), among a range of other applications (9, 62, 63). A recent example is adaptive drug therapy for metastatic castration-resistant prostate cancer (64, 65), which is currently being tested in a clinical trial (NCT02415621). The framework presented here could be translated into other disease sites or targetable mutations, however this would require recalibration of model parameters, which involved several studies as noted in Table 1. To recalibrate the model, the following literature obtained data is needed for the specific disease site: unrestricted tumor growth with time, failure rates after chemo/radiotherapy (both separately and together), failures rates after targeted therapy, and rates of non-cancerous failures (from SEER) (20, 21). With these data, along with literature estimates of pre-existing resistance and mutation rates, one could independently tune each model parameters as was done in a previous study (18).

Author Manuscript Author Manuscript Author Manuscript Author Manuscript

In conclusion, our mathematical framework provides an evolutionary argument against longer induction periods, as they could trigger the process of acquired drug resistance and may limit the efficacy of adjuvant therapy, possibly resulting in worse outcomes. According to our model a shorter induction period of 1–2 weeks had a greater chance of controlling TKI resistant cells with CRT, resulting in longer predicted progression free survival. Finally, the probability of observing a statistically significant increase in PFS due to a shorter induction period was stochastically derived as function of trial size, using randomly sampled heterogeneous patient populations. These model predictions are hypothesis generating and could have impact on clinical trial design. While this study has focused on optimizing TKI administration in combination with CRT for EGFR-mutant NSCLC, the generalized framework outlined in this paper can be applied to oncogene-driven multimodal therapy designs in other cancers.

Supplementary Material

Refer to Web version on PubMed Central for supplementary material.

Acknowledgments

This work was supported by grants from the NCI (CA21239 to Dr. Paganetti; CA197389 to Dr. Hata; and CA137008 to Dr. Sequist) and the American Lung Association (LCD-400286 to Dr. Willers).

Disclosure of Potential Conflicts of Interest:

A.N.H has received grants from Novartis, Amgen, Pfizer, Relay Therapeutics, Eli Lilly, Blueprint Medicines, and Roche/Genentech, all outside of the submitted work.

Z.P. has served as a compensated consultant or received honoraria from Blueprint, C4 Therapeutics, AstraZeneca, Spectrum, Ariad/Takeda, Novartis, ImmunoGen, AbbVie, GuardantHealth, Genentech, Eli Lilly, InCyte and Medtronic and has received grants from Novartis, Takeda, Spectrum, AstraZeneca, Tesaro, and Cullinan Oncology all outside of the submitted work.

L.V.S. has served as a compensated consultant or received honoraria from AstraZeneca, Genentech, Merrimack, and Janssen Oncology, has received grants from Boehringer Ingelheim, Genentech, Merrimack, Novartis, AstraZeneca, Blueprint Medicines, Loxo, and has a patent pending related to the treatment of EGFR-mutant lung cancer, all outside of the submitted work.

C.G. serves on the Scientific Advisory Board for Nanolive.

References

1. Rosell R, Carcereny E, Gervais R, Vergnenegre A, Massuti B, Felip E, Palmero R, Garcia-Gomez R, Pallares C, Sanchez JM, Porta R, Cobo M, Garrido P, Longo F, Moran T, Insa A, De Marinis F, Corre R, Bover I, Illiano A, Dansin E, de Castro J, Milella M, Reguart N, Altavilla G, Jimenez U, Provencio M, Moreno MA, Terrasa J, Munoz-Langa J, Valdivia J, Isla D, Domine M, Molinier O, Mazieres J, Baize N, Garcia-Campelo R, Robinet G, Rodriguez-Abreu D, Lopez-Vivanco G, Gebbia V, Ferrera-Delgado L, Bombaron P, Bernabe R, Bearz A, Artal A, Cortesi E, Rolfo C, Sanchez-Ronco M, Drozdowskyj A, Queralt C, de Aguirre I, Ramirez JL, Sanchez JJ, Molina MA, Taron M, Paz-Ares L, Spanish Lung Cancer Group in collaboration with Groupe Francais de P-C, Associazione Italiana Oncologia T. Erlotinib versus standard chemotherapy as first-line treatment for European patients with advanced EGFR mutation-positive non-small-cell lung cancer (EURTAC): a multicentre, open-label, randomised phase 3 trial. Lancet Oncol. 2012;13(3):239–46. doi: 10.1016/S1470-2045(11)70393-X. [PubMed: 22285168]
2. Soria JC, Ohe Y, Vansteenkiste J, Reungwetwattana T, Chewaskulyong B, Lee KH, Dechaphunkul A, Imamura F, Nogami N, Kurata T, Okamoto I, Zhou C, Cho BC, Cheng Y, Cho EK, Voon PJ,

Author Manuscript Author Manuscript Author Manuscript Author Manuscript

Planchard D, Su WC, Gray JE, Lee SM, Hodge R, Marotti M, Rukazenkov Y, Ramalingam SS, Investigators F. Osimertinib in Untreated EGFR-Mutated Advanced Non-Small-Cell Lung Cancer. N Engl J Med. 2018;378(2):113–25. doi: 10.1056/NEJMoa1713137. [PubMed: 29151359]

3. Ortiz-Cuaran S, Scheffler M, Plenker D, Dahmen L, Scheel AH, Fernandez-Cuesta L, Meder L, Lovly CM, Persigehl T, Merkelbach-Bruse S, Bos M, Michels S, Fischer R, Albus K, Konig K, Schildhaus HU, Fassunke J, Ihle MA, Pasternack H, Heydt C, Becker C, Altmuller J, Ji H, Muller C, Florin A, Heuckmann JM, Nuernberg P, Ansen S, Heukamp LC, Berg J, Pao W, Peifer M, Buettner R, Wolf J, Thomas RK, Sos ML. Heterogeneous Mechanisms of Primary and Acquired Resistance to Third-Generation EGFR Inhibitors. Clin Cancer Res. 2016;22(19):4837–47. doi: 10.1158/1078-0432.CCR-15-1915. [PubMed: 27252416]
4. Ramirez M, Rajaram S, Steininger RJ, Osipchuk D, Roth MA, Morinishi LS, Evans L, Ji W, Hsu CH, Thurley K, Wei S, Zhou A, Koduru PR, Posner BA, Wu LF, Altschuler SJ. Diverse drug-resistance mechanisms can emerge from drug-tolerant cancer persister cells. Nat Commun. 2016;7:10690 Epub 2016/02/20. doi: 10.1038/ncomms10690. [PubMed: 26891683]
5. Hata AN, Niederst MJ, Archibald HL, Gomez-Caraballo M, Siddiqui FM, Mulvey HE, Maruvka YE, Ji F, Bhang HE, Krishnamurthy Radhakrishna V, Siravegna G, Hu H, Raoof S, Lockerman E, Kalsy A, Lee D, Keating CL, Ruddy DA, Damon LJ, Crystal AS, Costa C, Piotrowska Z, Bardelli A, Iafrate AJ, Sadreyev RI, Stegmeier F, Getz G, Sequist LV, Faber AC, Engelman JA. Tumor cells can follow distinct evolutionary paths to become resistant to epidermal growth factor receptor inhibition. Nat Med. 2016;22(3):262–9. doi: 10.1038/nm.4040. [PubMed: 26828195]
6. Sequist LV, Waltman BA, Dias-Santagata D, Digumarthy S, Turke AB, Fidias P, Bergethon K, Shaw AT, Gettinger S, Cosper AK, Akhavanfard S, Heist RS, Temel J, Christensen JG, Wain JC, Lynch TJ, Vernovsky K, Mark EJ, Lanuti M, Iafrate AJ, Mino-Kenudson M, Engelman JA. Genotypic and histological evolution of lung cancers acquiring resistance to EGFR inhibitors. Sci Transl Med. 2011;3(75):75ra26. doi: 10.1126/scitranslmed.3002003.
7. Antonia SJ, Villegas A, Daniel D, Vicente D, Murakami S, Hui R, Yokoi T, Chiappori A, Lee KH, de Wit M, Cho BC, Bourhaba M, Quantin X, Tokito T, Mekhail T, Planchard D, Kim YC, Karapetis CS, Hiret S, Ostoros G, Kubota K, Gray JE, Paz-Ares L, de Castro Carpeno J, Wadsworth C, Melillo G, Jiang H, Huang Y, Dennis PA, Ozguroglu M, Investigators P. Durvalumab after Chemoradiotherapy in Stage III Non-Small-Cell Lung Cancer. N Engl J Med. 2017;377(20):1919–29. doi: 10.1056/NEJMoa1709937. [PubMed: 28885881]
8. Lee CK, Man J, Lord S, Links M, Gebski V, Mok T, Yang JC. Checkpoint Inhibitors in Metastatic EGFR-Mutated Non-Small Cell Lung Cancer-A Meta-Analysis. J Thorac Oncol. 2017;12(2):403–7. doi: 10.1016/j.jtho.2016.10.007. [PubMed: 27765535]
9. Altrock PM, Liu LL, Michor F. The mathematics of cancer: integrating quantitative models. Nat Rev Cancer. 2015;15(12):730–45. doi: 10.1038/nrc4029. [PubMed: 26597528]
10. Grassberger C, Scott JG, Paganetti H. Biomathematical Optimization of Radiation Therapy in the Era of Targeted Agents. Int J Radiat Oncol Biol Phys. 2017;97(1):13–7. doi: 10.1016/j.ijrobp.2016.09.008. [PubMed: 27979444]
11. Bozic I, Reiter JG, Allen B, Antal T, Chatterjee K, Shah P, Moon YS, Yaqubie A, Kelly N, Le DT, Lipson EJ, Chapman PB, Diaz LA Jr., Vogelstein B, Nowak MA. Evolutionary dynamics of cancer in response to targeted combination therapy. Elife. 2013;2:e00747. doi: 10.7554/eLife.00747. [PubMed: 23805382]
12. Grassberger C, McClatchy DM, Geng C, Kamran SC, Fintelmann F, Maruvka YE, Piotrowska Z, Willers H, Sequist LV, Hata AN, Paganetti H. Patient-specific tumor growth trajectories determine persistent and resistant cancer cell populations during treatment with targeted therapies. Cancer Research. 2019:canres.3652.2018. doi: 10.1158/0008-5472.CAN-18-3652.
13. Yoon N, Vander Velde R, Marusyk A, Scott JG. Optimal Therapy Scheduling Based on a Pair of Collaterally Sensitive Drugs. Bull Math Biol. 2018;80(7):1776–809. doi: 10.1007/s11538-018-0434-2. [PubMed: 29736596]
14. Leder K, Pitter K, LaPlant Q, Hambardzumyan D, Ross BD, Chan TA, Holland EC, Michor F. Mathematical modeling of PDGF-driven glioblastoma reveals optimized radiation dosing schedules. Cell. 2014;156(3):603–16. doi: 10.1016/j.cell.2013.12.029. [PubMed: 24485463]
15. Chmielecki J, Foo J, Oxnard GR, Hutchinson K, Ohashi K, Somwar R, Wang L, Amato KR, Arcila M, Sos ML, Socci ND, Viale A, de Stanchina E, Ginsberg MS, Thomas RK, Kris MG, Inoue A,

Author Manuscript Author Manuscript Author Manuscript Author Manuscript

Ladanyi M, Miller VA, Michor F, Pao W. Optimization of dosing for EGFR-mutant non-small cell lung cancer with evolutionary cancer modeling. Sci Transl Med. 2011;3(90):90ra59. doi: 10.1126/scitranslmed.3002356.

16. Yu HA, Sima C, Feldman D, Liu LL, Vaitheesvaran B, Cross J, Rudin CM, Kris MG, Pao W, Michor F, Riely GJ. Phase 1 study of twice weekly pulse dose and daily low-dose erlotinib as initial treatment for patients with EGFR-mutant lung cancers. Ann Oncol. 2017;28(2):278–84. doi: 10.1093/annonc/mdw556. [PubMed: 28073786]
17. Gao G, Ren S, Li A, Xu J, Xu Q, Su C, Guo J, Deng Q, Zhou C. Epidermal growth factor receptor-tyrosine kinase inhibitor therapy is effective as first-line treatment of advanced non-small-cell lung cancer with mutated EGFR: A meta-analysis from six phase III randomized controlled trials. Int J Cancer. 2012;131(5):E822–9. doi: 10.1002/ijc.27396. [PubMed: 22161771]
18. Geng C, Paganetti H, Grassberger C. Prediction of Treatment Response for Combined Chemo- and Radiation Therapy for Non-Small Cell Lung Cancer Patients Using a Bio-Mathematical Model. Sci Rep. 2017;7(1):13542. doi: 10.1038/s41598-017-13646-z. [PubMed: 29051600]
19. Yagishita S, Horinouchi H, Katsui Taniyama T, Nakamichi S, Kitazono S, Mizugaki H, Kanda S, Fujiwara Y, Nokihara H, Yamamoto N, Sumi M, Shiraishi K, Kohno T, Furuta K, Tsuta K, Tamura T. Epidermal growth factor receptor mutation is associated with longer local control after definitive chemoradiotherapy in patients with stage III nonsquamous non-small-cell lung cancer. Int J Radiat Oncol Biol Phys. 2015;91(1):140–8. doi: 10.1016/j.ijrobp.2014.08.344. [PubMed: 25442336]
20. Edwards BK, Noone AM, Mariotto AB, Simard EP, Boscoe FP, Henley SJ, Jemal A, Cho H, Anderson RN, Kohler BA, Eheman CR, Ward EM. Annual Report to the Nation on the status of cancer, 1975–2010, featuring prevalence of comorbidity and impact on survival among persons with lung, colorectal, breast, or prostate cancer. Cancer. 2014;120(9):1290–314. doi: 10.1002/cncr.28509. [PubMed: 24343171]
21. Cho H, Mariotto AB, Mann BS, Klabunde CN, Feuer EJ. Assessing non-cancer-related health status of US cancer patients: other-cause survival and comorbidity prevalence. Am J Epidemiol. 2013;178(3):339–49. doi: 10.1093/aje/kws580. [PubMed: 23825168]
22. Enewold L, Thomas A. Real-World Patterns of EGFR Testing and Treatment with Erlotinib for Non-Small Cell Lung Cancer in the United States. PLoS One. 2016;11(6):e0156728. doi: 10.1371/journal.pone.0156728. [PubMed: 27294665]
23. Lim YJ, Chang JH, Kim HJ, Keam B, Kim TM, Kim DW, Paeng JC, Kang KW, Chung JK, Jeon YK, Chung DH, Wu HG. Superior Treatment Response and In-field Tumor Control in Epidermal Growth Factor Receptor-mutant Genotype of Stage III Nonsquamous Non-Small cell Lung Cancer Undergoing Definitive Concurrent Chemoradiotherapy. Clin Lung Cancer. 2017;18(3):e169–e78. doi: 10.1016/j.cllc.2016.12.013. [PubMed: 28131636]
24. Mak RH, Doran E, Muzikansky A, Kang J, Neal JW, Baldini EH, Choi NC, Willers H, Jackman DM, Sequist LV. Outcomes after combined modality therapy for EGFR-mutant and wild-type locally advanced NSCLC. Oncologist. 2011;16(6):886–95. doi: 10.1634/theoncologist.2011-0040. [PubMed: 21632451]
25. Das AK, Sato M, Story MD, Peyton M, Graves R, Redpath S, Girard L, Gazdar AF, Shay JW, Minna JD, Nirodi CS. Non-small-cell lung cancers with kinase domain mutations in the epidermal growth factor receptor are sensitive to ionizing radiation. Cancer Res. 2006;66(19):9601–8. doi: 10.1158/0008-5472.CAN-06-2627. [PubMed: 17018617]
26. Thames HD, Bentzen SM, Turesson I, Overgaard M, Van den Bogaert W. Time-dose factors in radiotherapy: a review of the human data. Radiother Oncol. 1990;19(3):219–35. doi: 10.1016/0167-8140(90)90149-q. [PubMed: 2281152]
27. Switzer P, Gerstl B, Greenspoon J. Karyometry in the estimation of nuclear population in pulmonary carcinomas. J Natl Cancer Inst. 1974;52(6):1699–704. doi: 10.1093/jnci/52.6.1699. [PubMed: 4365386]
28. Cuaron J, Dunphy M, Rimner A. Role of FDG-PET scans in staging, response assessment, and follow-up care for non-small cell lung cancer. Front Oncol. 2012;2:208. doi: 10.3389/fonc.2012.00208. [PubMed: 23316478]
29. Williams MJ, Werner B, Barnes CP, Graham TA, Sottoriva A. Identification of neutral tumor evolution across cancer types. Nat Genet. 2016;48(3):238–44. doi: 10.1038/ng.3489. [PubMed: 26780609]

Author Manuscript Author Manuscript Author Manuscript Author Manuscript

30. Foo J, Chmielecki J, Pao W, Michor F. Effects of pharmacokinetic processes and varied dosing schedules on the dynamics of acquired resistance to erlotinib in EGFR-mutant lung cancer. J Thorac Oncol. 2012;7(10):1583–93. doi: 10.1097/JTO.0b013e31826146ee. [PubMed: 22982659]

31. Virtanen P, Gommers R, Oliphant TE, Haberland M, Reddy T, Cournapeau D, Burovski E, Peterson P, Weckesser W, Bright J, van der Walt SJ, Brett M, Wilson J, Millman KJ, Mayorov N, Nelson ARJ, Jones E, Kern R, Larson E, Carey CJ, Polat I, Feng Y, Moore EW, VanderPlas J, Laxalde D, Perktold J, Cimrman R, Henriksen I, Quintero EA, Harris CR, Archibald AM, Ribeiro AH, Pedregosa F, van Mulbregt P, SciPy C. SciPy 1.0: fundamental algorithms for scientific computing in Python. Nat Methods. 2020;17(3):261–72. Epub 2020/02/06. doi: 10.1038/s41592-019-0686-2. [PubMed: 32015543]

32. Oliphant TE. A guide to NumPy: Trelgol Publishing USA; 2006.

33. Waskom M, Botvinnik O, O'Kane D, Hobson P, Ostblom J, Lukauskas S, Gemperline DC, Augspurger T, Halchenko Y, Cole JB, Warmenhoven J, Ruiter Jd, Pye C, Hoyer S, Vanderplas J, Villalba S, Kunter G, Quintero E, Bachant P, Martin M, Meyer K, Miles A, Ram Y, Brunner T, Yarkoni T, Williams ML, Evans C, Fitzgerald C, Brian Qalieh A. mwaskom/seaborn: v0.9.0 (July 2018). v0.9.0 ed seaborn.pydata.org: Zenodo; 2018.

34. Davidson-Pilon C CamDavidsonPilon/lifelines: v0.24. v0.24 ed: Zenodo; 2020.

35. Senan S, Brade A, Wang LH, Vansteenkiste J, Dakhil S, Biesma B, Martinez Aguillo M, Aerts J, Govindan R, Rubio-Viqueira B, Lewanski C, Gandara D, Choy H, Mok T, Hossain A, Iscoe N, Treat J, Koustenis A, San Antonio B, Chouaki N, Vokes E. PROCLAIM: Randomized Phase III Trial of Pemetrexed-Cisplatin or Etoposide-Cisplatin Plus Thoracic Radiation Therapy Followed by Consolidation Chemotherapy in Locally Advanced Nonsquamous Non-Small-Cell Lung Cancer. J Clin Oncol. 2016;34(9):953–62. doi: 10.1200/JCO.2015.64.8824. [PubMed: 26811519]

36. Auperin A, Le Pechoux C, Rolland E, Curran WJ, Furuse K, Fournel P, Belderbos J, Clamon G, Ulutin HC, Paulus R, Yamanaka T, Bozonnat MC, Uitterhoeve A, Wang X, Stewart L, Arriagada R, Burdett S, Pignon JP. Meta-analysis of concomitant versus sequential radiochemotherapy in locally advanced non-small-cell lung cancer. J Clin Oncol. 2010;28(13):2181–90. doi: 10.1200/JCO.2009.26.2543. [PubMed: 20351327]

37. Komaki R, Allen PK, Wei X, Blumenschein GR, Tang X, Lee JJ, Welsh JW, Wistuba II, Liu DD, Hong WK. Adding Erlotinib to Chemoradiation Improves Overall Survival but Not Progression-Free Survival in Stage III Non-Small Cell Lung Cancer. Int J Radiat Oncol Biol Phys. 2015;92(2):317–24. doi: 10.1016/j.ijrobp.2015.02.005. [PubMed: 25968826]

38. Ready N, Janne PA, Bogart J, Dipetrillo T, Garst J, Graziano S, Gu L, Wang X, Green MR, Vokes EE, Cancer LGBCIL. Chemoradiotherapy and gefitinib in stage III non-small cell lung cancer with epidermal growth factor receptor and KRAS mutation analysis: cancer and leukemia group B (CALEB) 30106, a CALGB-stratified phase II trial. J Thorac Oncol. 2010;5(9):1382–90. doi: 10.1097/JTO.0b013e3181eba657. [PubMed: 20686428]

39. Solit DB, She Y, Lobo J, Kris MG, Scher HI, Rosen N, Sirotnak FM. Pulsatile administration of the epidermal growth factor receptor inhibitor gefitinib is significantly more effective than continuous dosing for sensitizing tumors to paclitaxel. Clin Cancer Res. 2005;11(5):1983–9. doi: 10.1158/1078-0432.CCR-04-1347. [PubMed: 15756024]

40. Gandara DR, Gumerlock PH. Epidermal growth factor receptor tyrosine kinase inhibitors plus chemotherapy: case closed or is the jury still out? J Clin Oncol. 2005;23(25):5856–8. doi: 10.1200/JCO.2005.05.030. [PubMed: 16043825]

41. Morgensztern D, Waqar S, Subramanian J, Gao F, Trinkaus K, Govindan R. Prognostic significance of tumor size in patients with stage III non-small-cell lung cancer: a surveillance, epidemiology, and end results (SEER) survey from 1998 to 2003. J Thorac Oncol. 2012;7(10):1479–84. doi: 10.1097/JTO.0b013e318267d032 [PubMed: 22982648]

42. Carmichael J, Degraff WG, Gamson J, Russo D, Gazdar AF, Levitt ML, Minna JD, Mitchell JB. Radiation sensitivity of human lung cancer cell lines. Eur J Cancer Clin Oncol. 1989;25(3):527–34. [PubMed: 2539297]

43. Magnuson WJ, Yeung JT, Guillod PD, Gettinger SN, Yu JB, Chiang VL. Impact of Deferring Radiation Therapy in Patients With Epidermal Growth Factor Receptor-Mutant Non-Small Cell Lung Cancer Who Develop Brain Metastases. Int J Radiat Oncol Biol Phys. 2016;95(2):673–9. doi: 10.1016/j.ijrobp.2016.01.037. [PubMed: 27034176]

Author Manuscript Author Manuscript Author Manuscript Author Manuscript

44. Wang M, Morsbach F, Sander D, Gheorghiu L, Nanda A, Benes C, Kriegs M, Krause M, Dikomey E, Baumann M, Dahm-Daphi J, Settleman J, Willers H. EGF receptor inhibition radiosensitizes NSCLC cells by inducing senescence in cells sustaining DNA double-strand breaks. Cancer Res. 2011;71(19):6261–9. doi: 10.1158/0008-5472.CAN-11-0213. [PubMed: 21852385]
45. Gerlinger M, Rowan AJ, Horswell S, Math M, Larkin J, Endesfelder D, Gronroos E, Martinez P, Matthews N, Stewart A, Tarpey P, Varela I, Phillimore B, Begum S, McDonald NQ, Butler A, Jones D, Raine K, Latimer C, Santos CR, Nohadani M, Eklund AC, Spencer-Dene B, Clark G, Pickering L, Stamp G, Gore M, Szallasi Z, Downward J, Futreal PA, Swanton C. Intratumor heterogeneity and branched evolution revealed by multiregion sequencing. N Engl J Med. 2012;366(10):883–92. doi: 10.1056/NEJMoa1113205. [PubMed: 22397650]
46. Clevers H The cancer stem cell: premises, promises and challenges. Nat Med. 2011;17(3):313–9. doi: 10.1038/nm.2304. [PubMed: 21386835]
47. Kreso A, Dick JE. Evolution of the cancer stem cell model. Cell Stem Cell. 2014;14(3):275–91. doi: 10.1016/j.stem.2014.02.006. [PubMed: 24607403]
48. Marusyk A, Tabassum DP, Altrock PM, Almendro V, Michor F, Polyak K. Non-cell-autonomous driving of tumour growth supports sub-clonal heterogeneity. Nature. 2014;514(7520):54–8. Epub 2014/08/01. doi: 10.1038/nature13556. [PubMed: 25079331]
49. Kaznatcheev A, Peacock J, Basanta D, Marusyk A, Scott JG. Fibroblasts and alectinib switch the evolutionary games played by non-small cell lung cancer. Nat Ecol Evol. 2019;3(3):450–6. Epub 2019/02/20. doi: 10.1038/s41559-018-0768-z. [PubMed: 30778184]
50. Seto T, Kato T, Nishio M, Goto K, Atagi S, Hosomi Y, Yamamoto N, Hida T, Maemondo M, Nakagawa K, Nagase S, Okamoto I, Yamanaka T, Tajima K, Harada R, Fukuoka M, Yamamoto N. Erlotinib alone or with bevacizumab as first-line therapy in patients with advanced non-squamous non-small-cell lung cancer harbouring EGFR mutations (JO25567): an open-label, randomised, multicentre, phase 2 study. Lancet Oncol. 2014;15(11):1236–44. doi: 10.1016/S1470-2045(14)70381-X. [PubMed: 25175099]
51. Liccardi G, Hartley JA, Hochhauser D. Importance of EGFR/ERCC1 interaction following radiation-induced DNA damage. Clin Cancer Res. 2014;20(13):3496–506. Epub 2014/05/02. doi: 10.1158/1078-0432.CCR-13-2695. [PubMed: 24780295]
52. Liccardi G, Hartley JA, Hochhauser D. EGFR nuclear translocation modulates DNA repair following cisplatin and ionizing radiation treatment. Cancer Res. 2011;71(3):1103–14. Epub 2011/01/27. doi: 10.1158/0008-5472.CAN-10-2384. [PubMed: 21266349]
53. Wu YL, Lee JS, Thongprasert S, Yu CJ, Zhang L, Ladrera G, Srimuninnimit V, Sriuranpong V, Sandoval-Tan J, Zhu Y, Liao M, Zhou C, Pan H, Lee V, Chen YM, Sun Y, Margono B, Fuerte F, Chang GC, Seetalarom K, Wang J, Cheng A, Syahruddin E, Qian X, Ho J, Kurnianda J, Liu HE, Jin K, Truman M, Bara I, Mok T. Intercalated combination of chemotherapy and erlotinib for patients with advanced stage non-small-cell lung cancer (FASTACT-2): a randomised, double-blind trial. Lancet Oncol. 2013;14(8):777–86. doi: 10.1016/S1470-2045(13)70254-7. [PubMed: 23782814]
54. Guo T, Ni J, Yang X, Li Y, Li Y, Zou L, Wang S, Liu Q, Chu L, Chu X, Li S, Ye L, Zhu Z. Pattern of Recurrence Analysis in Metastatic EGFR-Mutant NSCLC Treated with Osimertinib: Implications for Consolidative Stereotactic Body Radiation Therapy. Int J Radiat Oncol Biol Phys. 2020 Epub 2020/01/29. doi: 10.1016/j.ijrobp.2019.12.042.
55. Schiller JH, Harrington D, Belani CP, Langer C, Sandler A, Krook J, Zhu J, Johnson DH, Eastern Cooperative Oncology G. Comparison of four chemotherapy regimens for advanced non-small-cell lung cancer. N Engl J Med. 2002;346(2):92–8. doi: 10.1056/NEJMoa011954. [PubMed: 11784875]
56. Qiao GB, Wu YL, Yang XN, Zhong WZ, Xie D, Guan XY, Fischer D, Kolberg HC, Kruger S, Stuerzbecher HW. High-level expression of Rad51 is an independent prognostic marker of survival in non-small-cell lung cancer patients. Br J Cancer. 2005;93(1):137–43. doi: 10.1038/sj.bjc.6602665. [PubMed: 15956972]
57. Torres-Roca JF, Eschrich S, Zhao H, Bloom G, Sung J, McCarthy S, Cantor AB, Scuto A, Li C, Zhang S, Jove R, Yeatman T. Prediction of radiation sensitivity using a gene expression classifier. Cancer Res. 2005;65(16):7169–76. doi: 10.1158/0008-5472.CAN-05-0656. [PubMed: 16103067]

Author Manuscript Author Manuscript Author Manuscript Author Manuscript

58. Scott JG, Berglund A, Schell MJ, Mihaylov I, Fulp WJ, Yue B, Welsh E, Caudell JJ, Ahmed K, Strom TS, Mellon E, Venkat P, Johnstone P, Foekens J, Lee J, Moros E, Dalton WS, Eschrich SA, McLeod H, Harrison LB, Torres-Roca JF. A genome-based model for adjusting radiotherapy dose (GARD): a retrospective, cohort-based study. Lancet Oncol. 2017;18(2):202–11. doi: 10.1016/S1470-2045(16)30648-9. [PubMed: 27993569]

59. Chalkidou A, Landau DB, Odell EW, Cornelius VR, O'Doherty MJ, Marsden PK. Correlation between Ki-67 immunohistochemistry and 18F-fluorothymidine uptake in patients with cancer: A systematic review and meta-analysis. Eur J Cancer. 2012;48(18):3499–513. doi: 10.1016/j.ejca.2012.05.001. [PubMed: 22658807]

60. Rockne RC, Hawkins-Daarud A, Swanson KR, Sluka JP, Glazier JA, Macklin P, Hormuth DA, Jarrett AM, Lima E, Tinsley Oden J, Biros G, Yankeelov TE, Curtius K, Al Bakir I, Wodarz D, Komarova N, Aparicio L, Bordyuh M, Rabadan R, Finley SD, Enderling H, Caudell J, Moros EG, Anderson ARA, Gatenby RA, Kaznatcheev A, Jeavons P, Krishnan N, Pelesko J, Wadhwa RR, Yoon N, Nichol D, Marusyk A, Hinczewski M, Scott JG. The 2019 mathematical oncology roadmap. Phys Biol. 2019;16(4):041005. doi: 10.1088/1478-3975/ab1a09. [PubMed: 30991381]

61. Werner B, Scott JG, Sottoriva A, Anderson AR, Traulsen A, Altrock PM. The Cancer Stem Cell Fraction in Hierarchically Organized Tumors Can Be Estimated Using Mathematical Modeling and Patient-Specific Treatment Trajectories. Cancer Res. 2016;76(7):1705–13. doi: 10.1158/0008-5472.CAN-15-2069. [PubMed: 26833122]

62. Grassberger C, Ellsworth SG, Wilks MQ, Keane FK, Loeffler JS. Assessing the interactions between radiotherapy and antitumour immunity. Nat Rev Clin Oncol. 2019;16(12):729–45. doi: 10.1038/s41571-019-0238-9. [PubMed: 31243334]

63. Walker R, Enderling H. From concept to clinic: Mathematically informed immunotherapy. Curr Probl Cancer. 2016;40(1):68–83. doi: 10.1016/j.currproblcancer.2015.10.004. [PubMed: 26645497]

64. Zhang J, Cunningham JJ, Brown JS, Gatenby RA. Integrating evolutionary dynamics into treatment of metastatic castrate-resistant prostate cancer. Nat Commun. 2017;8(1):1816. doi: 10.1038/s41467-017-01968-5. [PubMed: 29180633]

65. West JB, Dinh MN, Brown JS, Zhang J, Anderson AR, Gatenby RA. Multidrug Cancer Therapy in Metastatic Castrate-Resistant Prostate Cancer: An Evolution-Based Strategy. Clin Cancer Res. 2019;25(14):4413–21. doi: 10.1158/1078-0432.CCR-19-0006. [PubMed: 30992299]

Author Manuscript Author Manuscript Author Manuscript Author Manuscript

Significance

A bio-mathematical framework based on fundamental principles of evolution and radiobiology for in silico clinical trial design allows clinicians to optimize administration of tyrosine kinase inhibitors before chemoradiotherapy in oncogene-driven NSCLC.

Author Manuscript Author Manuscript Author Manuscript Author Manuscript

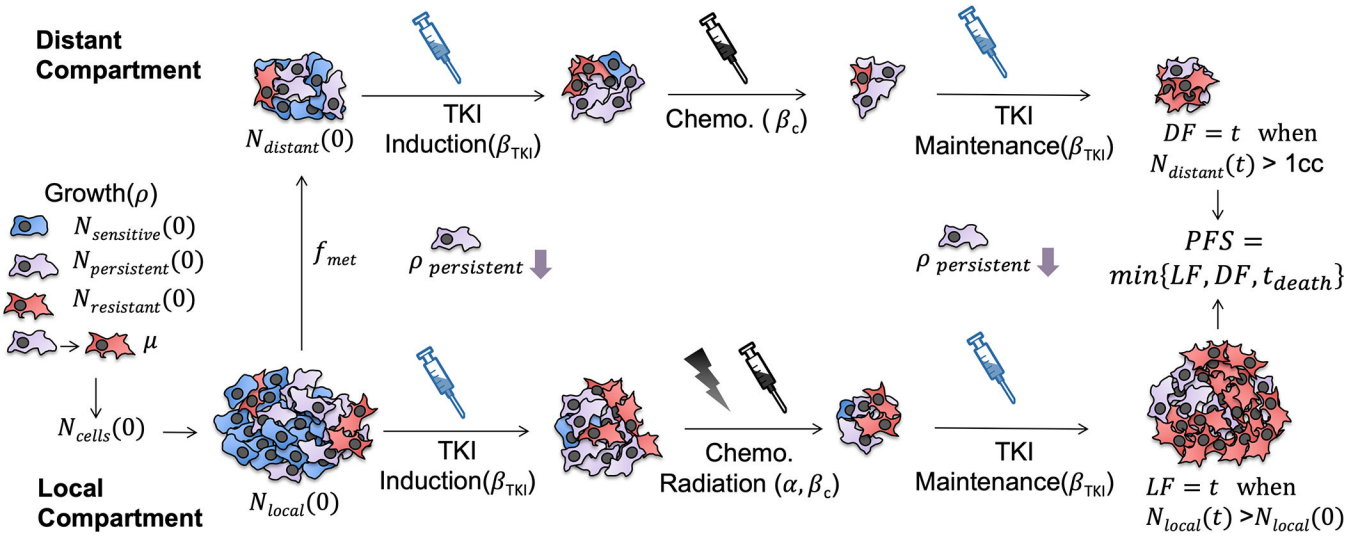

Figure 1:

Graphical illustration of the distant and local tumor progression model. TKI sensitive, persistent, and resistant cells are shaded blue, purple, and red, respectively. The distant tumor compartment (top) is only susceptible to systemic agents, in this case chemotherapy and TKI therapy. The local tumor compartment (bottom) is additionally affected by radiation therapy. Note that TKI therapy is not only specific to sensitive cells but also leads to slowed growth of persistent cells, as depicted by the downward purple arrow in the illustration. Chemo-radiation however is assumed to have equal effects on each cell subpopulation. The initial number of distant cells is assumed to be a constant fraction of the cells in the initial primary tumor.

Author Manuscript Author Manuscript Author Manuscript Author Manuscript

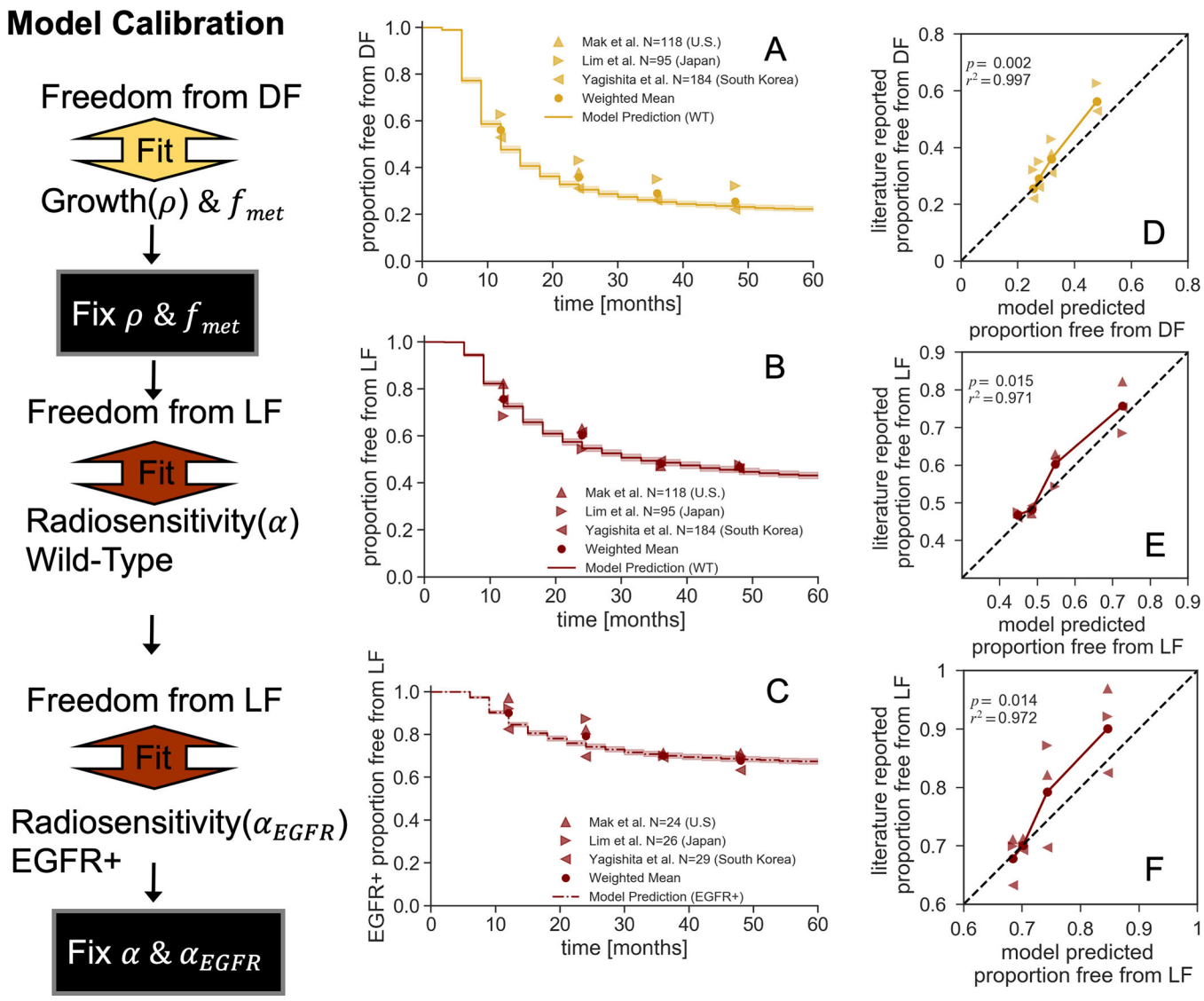

Figure 2 –. Model Calibration:

(A-C) Simulated freedom from distant (A) and local (B, WT and C, EGFR-mutant) failure Kaplan-Meier curves using the calibrated model parameters. (D-F) Corresponding model predicted versus literature reported failure rates at 1, 2, 3, and 4 yr. time points. The solid line represents the model predicted versus the weighted mean of literature reported failures, with corresponding linear regression and summary statistics. The black dashed line represents unity.

Author Manuscript
Author Manuscript
Author Manuscript
Author Manuscript

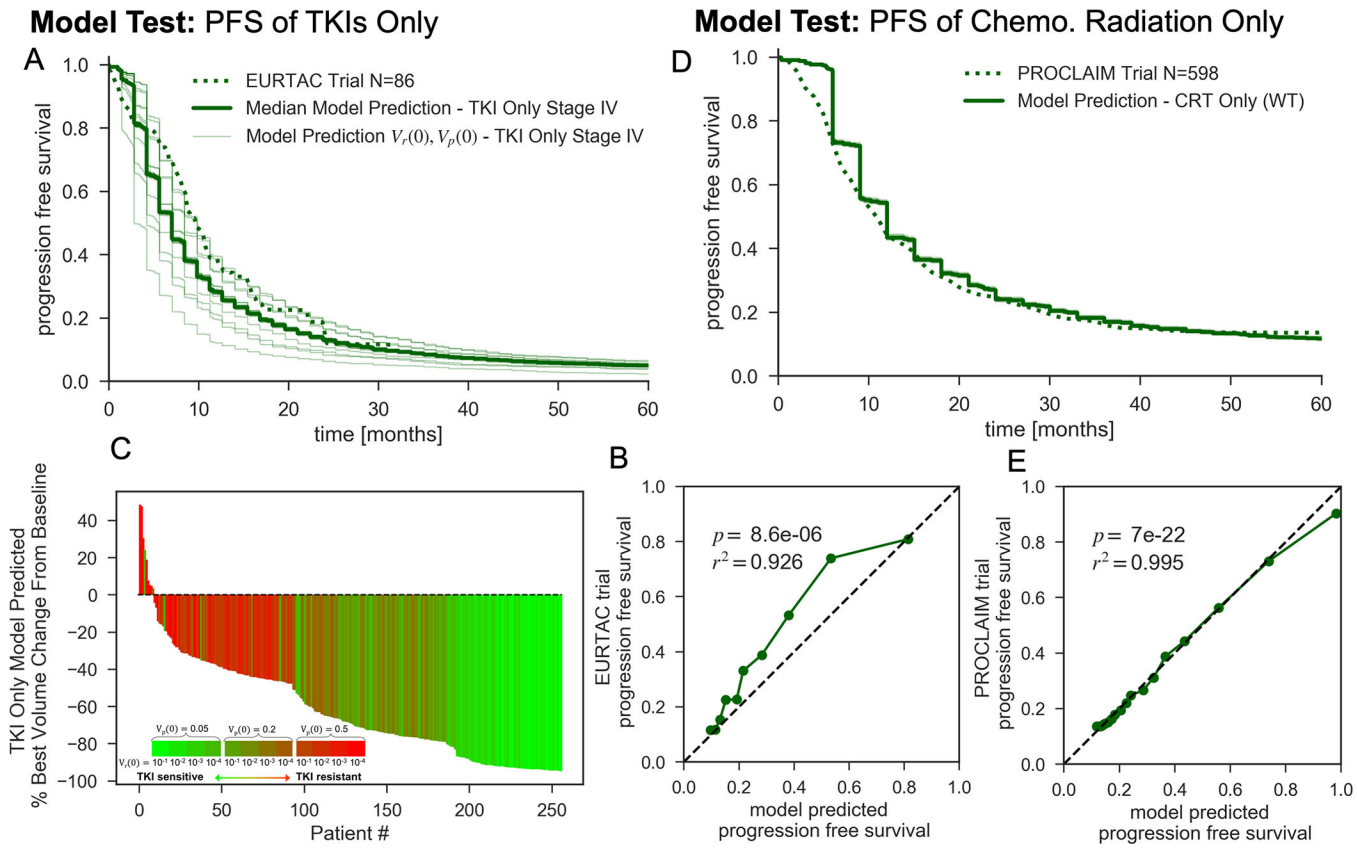

Figure 3 –. Model Validation:

(A) Model predicted and trial reported PFS K-M curves for stage IV, EGFR-mutant NSCLC populations receiving TKIs until progression. The 12 thin K-M curves represent each initial starting persistent and resistant fraction combination (see Suppl. Note), while the full line is the aggregate response. (B) Plot of model predicted versus trial reported PFS over 3 month intervals corresponding to (A) with linear regression summary statistics and the black dashed line representing unity. (C) Waterfall plot of best model predicted volume change from baseline for stage IV, EGFR-mutant NSCLC populations receiving TKIs until progression for a random subset of 256 modeled patients, color-coded by the 12 initial TKI persistence/resistance conditions. (D) Model predicted and trial reported PFS K-M curves for stage III NSCLC populations receiving definitive CRT, with a corresponding plot of model predicted versus trial reported PFS over 3 month intervals and summary statistics in (E).

Author Manuscript Author Manuscript Author Manuscript Author Manuscript

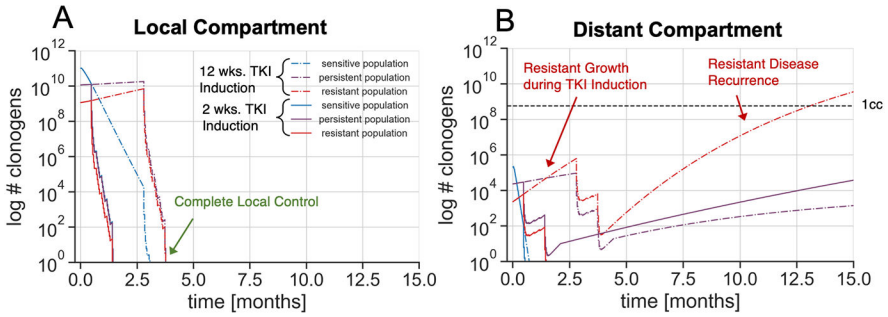

C

Induction Length	Hazard Ratios (95 CIs) vs CRT only		
	FFLF	FFDF	PFS
2 wks.	1.25 (1.20-1.31)	1.89 (1.83-1.96)	1.74 (1.69-1.80)
8 wks.	1.21 (1.15-1.26)	1.48 (1.43-1.52)	1.44 (1.39-1.48)
12 wks.	1.19 (1.14-1.25)	1.38 (1.34-1.43)	1.38 (1.34-1.42)

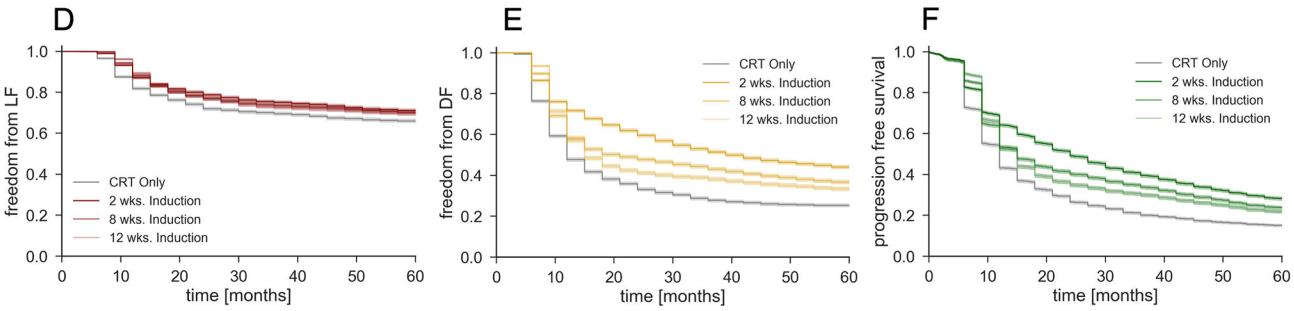

Figure 4 –. Model Predictions for Variable Induction Periods:

Model predicted freedom from local failure (D), freedom from distant failure (E), and progression free survival (F) K-M curves for various induction lengths. The simulated treatment regimen is TKI induction, chemoradiotherapy, and adjuvant TKI maintenance. The local and distant tumor volume trajectory of the median simulated patient with an initial persistent fraction of 0.1 and initial resistant fraction of 0.01, stratified by TKI response cell subtypes, are shown in (A) and (B) respectively. Hazard ratios corresponding to the K-M curves (D-F) are shown in (C).

Author Manuscript
Author Manuscript
Author Manuscript
Author Manuscript

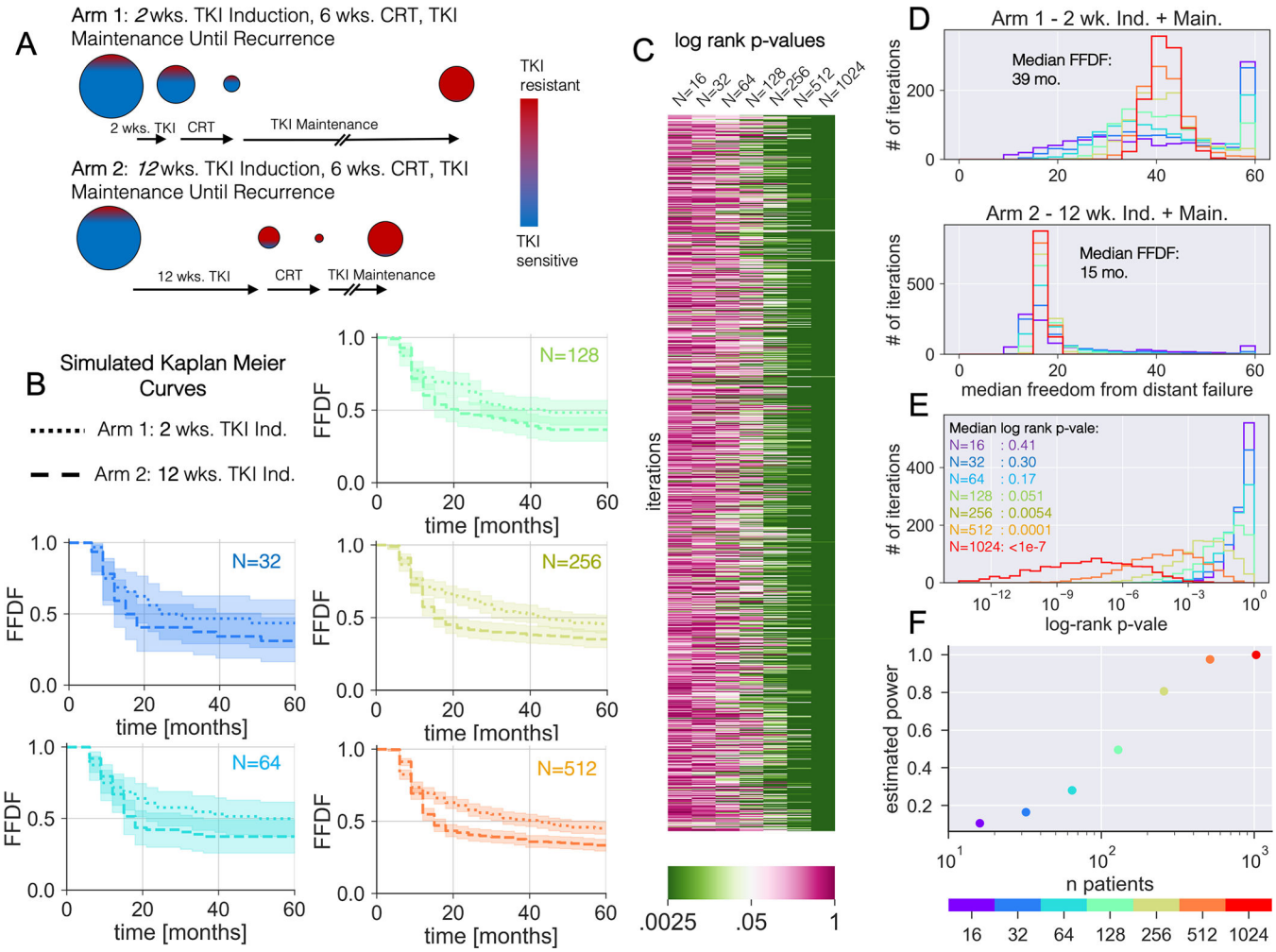

Figure 5 –. Simulated *in-silico* Induction Trial:

(A) Illustration of the differential evolution of the TKI resistant and sensitive populations for a given tumor burden between a short 2 wk. and long 12 wk. induction length. When CRT is done after a significant TKI induction period, the tumor shrinks with the targeted drug killing the TKI sensitive cells (blue), but with more TKI resistant (red) cells at the time of CRT, increasing the chance of a late TKI resistant recurrence if CRT isn't curative. (B) Simulated FFDF K-M curves for 2 wk. versus 12 wk. induction lengths with increasing number of simulated patients. Each curve corresponds to the iteration with the median log-rank p-vale. (C) A heatmap of log rank p-values testing statistical difference between the 2 wk. versus 12 wk. FFDF K-M curves for 1000 iterations of the simulation at each sample size. (D) Histograms of the median FFDF for the 1000 iterations of the 2 wk. and 12 wk. induction simulations at each sample size. (E) Histogram of the log rank p-value between the 2 wk. versus 12 wk. induction simulations at each sample size. (F) Estimated statistical power as a function of sample size. Here statistical power was estimated as the fraction of iteration resulting in a p-value<0.05.

Author Manuscript Author Manuscript Author Manuscript Author Manuscript

Table 1 –

Parameter Overview: Overview of key model parameters along with data sources used for model calibration and testing. Units in brackets, distributions in curly brackets, and 95% confidence intervals in parentheses for parameters fitted in this work.

Key Model Parameters – Estimated From Literature & Previous Studies			
Parameter	Description	Value	Source
$N_{cells}(0)$	initial number of local clonogens	$[9.1*10^6 – 6.7*10^{11}]$ **[**cells**]**	Geng et al.[18]
K	gompertzian carrying capacity	$8.2*10^{12}$ **[**cells**]**	Geng et al.[18]
$V_p(0) = N_{persistent}(0)/N_{cells}(0)$ $V_r(0) = N_{persistent}(0)/N_{cells}(0)$	initial fraction of TKI persistent & TKI resistant clonogens	[0.05 – 0.5] **[-]** $[10^{-4} – 10^{-1}]$ **[-]**	Grassberger et al.[12]
μ	resistant mutation probability	10^{-7} **[-]**	Grassberger et al.[12]
β_{TKI}	TKI cell kill parameter	trunc-norm {μ=2, σ=7} **[**ml/μg**]**; (>1)	Grassberger et al.[12]
β_c	chemotherapy cell kill parameter	trunc-norm {μ=.028, $\sigma=6.8*10^{-4}$} **[**m^2/mg**]**; (>0)	Geng et al.[18]
$t_{1/2}$	chemotherapy plasma half life	24 **[**hr**]**	Geng et al.[18]
κ	TKI plasma decay factor	0.0465 **[**hr^{-1}**]**	Grassberger et al.[12], Foo et al.[30]
r_{death}	comorbidity death rate for regional lung cancer	0.55 **[**%/mo**]**	SEER[20, 21]
Key Model Parameters – Derived In Current Study			
Parameter	Description	Value	Source
f_{met}	initial number of metastatic clonogens as a fraction of $N_{cells}(0)$	$2*10^{-6}$ **(CI:** $7.5*10^{-7} – 4*10^{-6}$**) [-]**	this work
ρ	NSCLC growth rate	trunc-norm {$\mu=7*10^{-5}$, σ=.0055 **(CI:** .005–.007**)**} **[**day^{-1}**]**; (>0)	this work
α	WT NSCLC radiosensitivity	trunc-norm {μ=.10 **(CI:** .04–.18**)**, σ=.17 **(CI:** .11–.2**)**} **[**Gy^{-1}**]**; (>0)	this work
α_{EGFR}	EGFR-mutant NSCLC radiosensitivity	trunc-norm {μ=.16 **(CI:** .10–.26**)**, σ=.32 **(CI:** .20–.44**)**} **[**Gy^{-1}**]**; (>0)	this work
Clinical Data used for Calibrating & Testing Model In Current Study			
Dataset	Description	Endpoint	Source
Calibration (N=118, USA)	institutional LF & DF rates in EGFR-mutant/WT LA-NSCLC	FFLF & FFDF **[**mo**]**	Mak et al.[24]
Calibration (N=95, Japan)	institutional LF & DF rates in EGFR-mutant /WT LA-NSCLC	FFLF & FFDF **[**mo**]**	Lim et al.[23]
Calibration (N=185, S. Korea)	institutional LF & DF rates in EGFR-mutant /WT LA-NSCLC	FFLF & FFDF **[**mo**]**	Yagishita et al.[19]
Testing (N=86, France, Italy, Spain)	phase III clinical trial of TKIs in metastatic NSCLC (NCT00446225)	PFS **[**mo**]**	EURTAC Trial, Rosell et al.[1]
Testing (N=598, Worldwide)	phase III clinical trial of concurrent chemoradiation in locally advanced NSCLC (NCT00686959)	PFS **[**mo**]**	PROCLAIM Trial, Senan et al.[35]

Testing (N=6 Clinical Trials)	meta-analysis of 6 clinical trials of sequential versus concurrent chemoradiotherapy in LA-NSCLC	FFLF & FFDF [mo]	Auperin et al.[36]

Author Manuscript
Author Manuscript
Author Manuscript
Author Manuscript